Limits on the Short Term Variability of Sagittarius A* in the Near-Infrared

S.D. Hornstein[1], A.M. Ghez[1,2], A. Tanner[1], M. Morris[1], E.E. Becklin[1], P. Wizinowich[3]

ABSTRACT

The recent detection of a 3-hr X-ray flare by the Chandra Observatory has raised the possibility of enhanced emission over a broad range of wavelengths from Sgr A*, the suspected 2.6 x 10^6 $M_\odot$ black hole at the Galactic Center, during a flaring event. We have, therefore, reconstructed 3-hr data sets from 2μm speckle and adaptive optics images (θ_{core} = 50 - 100 mas) obtained with the W. M. Keck 10-m telescopes between 1995 and 2001. In 25 separate observations, no evidence of any significant excess emission associated with Sgr A* was detected. The lowest of our detection limits gives an observed limit for the quiescent state of Sgr A* of 0.09$\pm$0.005 mJy, or, equivalently, a dereddened value of 2.0$\pm$0.1 mJy, which is a factor of 2 lower than the best previously published quiescent value. Under the assumption that there are random 3-hr flares producing both enhanced X-ray and near-infrared emission, our highest limit constrains the variable state of Sgr A* to $\lesssim$0.8 mJy (observed) or 19 mJy (dereddened). These results suggest that the model favored by Markoff et al. (2001), in which the flare is produced through local heating of relativistic particles surrounding Sgr A* (e.g., a sudden magnetic reconnection event), is unlikely, because it predicts peak 2μm emission of $\sim$300 mJy, well above our detection limit.

Subject headings: Galaxy: center — infrared: galaxies — X-rays: galaxies — accretion, accretion disks — galaxies: jets — black hole physics

1. Introduction

The variability of Sagittarius (Sgr) A* at X-ray wavelengths (Baganoff et al. 2001a) has bolstered the case for associating this source with the suspected 2.6 x 10^6 $M_\odot$ black hole at

[1]Department of Physics and Astronomy, University of California, Los Angeles, CA 90095-1562

[2]Institute for Geophysics and Planetary Physics, University of California, Los Angeles, CA 90095-1565

[3]W.M. Keck Observatory, 65-1120 Mamalahoa Hwy., Kamuela, HI 96743

the center of our Galaxy (Eckart & Genzel 1997; Genzel et al. 1997, 2000; Ghez et al. 1998, 2000). In two Chandra observations separated by almost a year and having a total of 76 ksec of exposure time, Sgr A* was detected at X-ray wavelengths for the first time and was also seen to flare in intensity over a time scale of 3 hours (Baganoff et al. 2001a,b). While the flare's short duration implied a small region of origin, $\lesssim$400 R_s (where R_s is the Schwarzschild radius = $2GM_\bullet/c^2$), its large amplitude, a factor of 50, has raised the possibility of detecting corresponding intensity enhancements at wavelengths outside the X-ray regime.

Existing models for Sgr A*'s flared state make very disparate predictions for the emission at wavelengths between the X-ray and radio regimes (Markoff et al. 2001; Liu & Melia 2002). The wide differences between these models are a result of assuming different geometries (disk vs. jet) and emission mechanisms for the flaring process (e.g., enhanced accretion rates vs. magnetic reconnection). In some models, the predicted emission in the flared state, at infrared (IR) wavelengths, dramatically exceeds that of existing detection limits (Genzel & Eckart 1999; Stolovy et al. 1999; Morris et al. 2001). For example, the preferred model of Markoff et al. (2001) predicts an observed 2μm flux density of ~13 mJy, or a dereddened flux density of ~300 mJy, during the flared state. Unlike the situation at radio wavelengths, where long-term monitoring campaigns have been used to constrain the flared state of Sgr A* (Zhao, Bower, & Goss 2001), the limited time coverage and spatial resolution of published IR experiments prevent meaningful constraints on the flared state's IR emission from being inferred[4] and, thus, the reported limits are assumed to be associated with Sgr A*'s quiescent state.

The W. M. Keck Observatory dynamical study of stars in the central stellar cluster (Ghez et al. 1998, 2000; Gezari et al. 2002) provides a rich source of high angular resolution 2μm data between 1995 and 2001. In this paper, we present 2μm flux density limits from maps that were each composed of data from a single night. The elapsed time of 3-4 hours in each map is approximately the same as the time scale of the observed X-ray flare, making this data set ideally suited for possibly detecting a flare of this type. Given the quantity of these observations, our non-detections establish a robust upper limit for the flared state's 2μm emission intensity.

---

[4]While several papers have reported the possible detection of a variable near-infrared source coincident with Sgr A* (Herbst, Beckwith, & Shure 1993; Close, McCarthy, & Melia 1995; Genzel et al. 1997), subsequent high resolution observations have identified this emission to be from high proper motion sources (Eckart et al. 1995; Eckart & Genzel 1997; Ghez et al. 1998, 2002).

2. Observations

High resolution, near-infrared observations of the Galactic Center were conducted from 1995 June to 2001 July using both speckle and adaptive optics (AO) imaging techniques on the Keck 10-m telescopes. The speckle observations were obtained in the K-band (λ_o = 2.2μm, $\Delta\lambda$=0.4μm) using the Keck I facility near-infrared camera (NIRC; Matthews & Soifer 1994) with external re-imaging optics. This resulted in a pixel scale of $0\overset{''}{.}0203$ and a field of view (FOV) of $5\overset{''}{.}12\times5\overset{''}{.}12$ (Matthews et al. 1996). During each night of observations several thousand short exposures (t_{exp}= 0.137 sec) were taken in sets of $\sim$200. A more limited set of data was collected using two different science cameras behind the Keck II AO system (Wizinowich 2000). The first AO data set was collected in the K'-band (λ_o = 2.1μm, $\Delta\lambda$=0.35μm) in early 1999 with the near-infrared engineering camera (KCAM; Wizinowich et al. 2000), which had a pixel scale of $0\overset{''}{.}0175$, a FOV of $4\overset{''}{.}4\times4\overset{''}{.}4$. Each image had an exposure time of 5 sec. The slit-viewing camera of NIRSPEC (SCAM; McLean et al. 1998) provided a second set of AO images for this study. These images, like the speckle images, were made in the K-band and have a pixel scale of $0\overset{''}{.}0170$ and a FOV of $4\overset{''}{.}4\times4\overset{''}{.}4$, and exposure time of 10 sec. USNO 0600-28579500 served as the natural guide star for all of these AO observations. Since this guide star is both faint (R = 13.2) and distant from the target (r$\sim$30$''$), the AO performance was non-optimal. Table 1 provides a summary of all observations.

3. Data Analysis & Results

Three basic steps constitute the data analysis process in this program. First, high angular resolution maps are generated from the individual short exposure frames (§3.1). Second, all point sources in the FOV are identified and a direct detection of Sgr A* is ruled out (§3.2). Third, limits for Sgr A* are derived from the residual maps, in which all identified point sources have been removed (§3.3).

3.1. Construction of Images

Image processing proceeds similarly to that carried out for the dynamical experiment with one exception. Rather than combining all the data from the duration of an observing run, typically 2-3 nights, we synthesize the data over each night to produce 27 maps, each of which is limited to an elapsed time of 3-4 hours. Since the details of this method are described elsewhere (Ghez et al. 1998), only a brief summary is provided here. Standard image reduction techniques are applied to all the individual speckle and AO frames. For the speckle data, a two stage shift-and-add (SAA; Christou 1991; Ghez et al. 1998) analysis then produces the final high resolution maps. In the first stage, the 200 frames in each set are combined to form an intermediate SAA image. Then, these multiple intermediate SAA images (from throughout the night) are combined to form one final SAA map. This allows each intermediate image to be examined for seeing quality. In combining the intermediate images, a seeing cut is established so as to exclude those images with the worst seeing from the final map. For the AO data, this cut is also carried out on the individual AO images before they are registered and averaged together. Figure 1 displays representative final nightly speckle and AO maps.

3.2. Point Source Identification & Search for Sgr A*'s near-infrared emission

In all maps, stars are identified using StarFinder, an IDL package developed for astrometry and photometry in crowded stellar fields (Diolaiti et al. 2000). This package iteratively generates estimates of the point spread function (PSF) from a few selected bright stars and then identifies point sources over the entire FOV through cross-correlation of the map with the PSF model. For the PSF extraction, we found that the most reliable PSF models are obtained with a support size of $\sim 2''$, which represents a compromise between needing to accommodate the large PSF halos and yet having a limited FOV. This choice limits our analysis to images with PSF halo sizes of $0\farcs4$ or less, as the PSFs of the remaining two images are poorly characterized by this process. The PSF model is based on four of the five brightest stars in the FOV (IRS 16NE, 16C, 16NW, and 29N; see Figure 1); IRS 16SW is avoided as a PSF model star, since it is surrounded by relatively bright stars in its immediate vicinity. For point source identification, a correlation coefficient greater than 0.8 between the PSF model and the actual stellar image is required to avoid spurious detections. This process results in the identification of $\sim$100 point sources in each map.

The speckle and AO images have significantly different PSFs. Nonetheless, both PSFs are composed of a compact core on top of a broader halo. Table 1 provides the characterization of the PSF in each map based on the radial profile of the PSF model. While the speckle images have PSF core FWHM that are nearly diffraction limited ($\sim 0\farcs05$) and $\sim$40% smaller than that of the AO images ($\sim 0\farcs08$), the AO PSF core contains $\sim$30% of the total energy, $\sim$12 times more than the typical speckle PSF.

At this stage in the analysis, it is possible to look for direct detections of Sgr A*. We use proper motion acceleration vectors (Ghez et al. 2000) to pinpoint the central black hole's position relative to the nominal radio position of Sgr A* (Menten et al. 1997) to within $0\farcs04$

(1σ). Within $0\farcs08$ of this location, 4 sources ($13.9 < \mathrm{K} < 16.5$) are identified, all of which were previously detected in "monthly" maps made from all data in a single observing run (Ghez et al. 1998, 2002) and, furthermore, have significant proper motions. This high stellar density emphasizes the need for improved accuracy in Sgr A*'s position in the IR reference frame in order to measure or constrain its emission. With no stationary source identified in this region, we conclude that Sgr A* has not been detected.

3.3. Flux Density Limits for Sgr A*

In order to determine an accurate detection limit at the position of Sgr A*, it is necessary to remove the contaminating seeing halos from nearby sources. A 'stars only' map is created using the PSF model and list of stars generated by StarFinder. This is then subtracted from the original map, producing a residual map. With the residual map, a 3σ point source detection limit for Sgr A* is established based on three times the RMS of 25 aperture photometry values, which are calculated using $\sim$60 mas radius apertures and sky annuli extending from $\sim$60 mas to $\sim$90 mas. The 5$\times$5 grid of apertures in the residual map corresponds to an area of $\sim 0\farcs6 \times 0\farcs6$, more than two orders of magnitude larger than the uncertainty in the location of Sgr A*.

Zero points are obtained through carrying out the same aperture photometry in the original maps (prior to the 'stars only' subtraction) on all known non-variable sources brighter than K=10.5,using the flux densities reported in Blum, Sellgren, & Depoy (1996), and that occur in more than 30% of the frames for each night. The photometric calibration sources used are IRS 16NW, 16C, 16CC, and 16NE, when the FOV allows its inclusion; IRS 29N is omitted as it is found to be marginally variable at the 2σ level. Typical photometric zero point 1σ uncertainties of $\sim$0.04 mag result from this procedure.

Table 1 and Figure 2 contain the resulting 3σ point source detection limits for Sgr A*. The lowest of these upper limits gives an observed limit for the quiescent state of Sgr A* of 0.09$\pm$0.005 mJy, or, equivalently, a dereddened value of 2.0$\pm$0.1 mJy, while the highest limit constrains our analysis of the variable state of Sgr A* to $\lesssim$0.8 mJy (observed) or 19 mJy (dereddened). Although these upper limits vary significantly from epoch to epoch (due to variable observing conditions and/or a variation in the number of contaminating sources detected and removed) the lowest of them is lower than the best previously reported limits at 2μm for Sgr A*'s quiescent state (dereddened 4 mJy; Genzel & Eckart 1999) by a factor of 2.

4. Discussion

Using the coverage of the X-ray and near-infrared experiments and assuming random 3-hr flaring events that produce both enhanced X-ray and near-infrared emission, we consider the likelihood that a near-infrared flare in excess of our weakest limit occurred over the course of the IR experiment. The probability of seeing such a flare is given by the following binomial distribution:

$$P(\nu \text{ detections in } n \text{ trials}) = \frac{n!}{\nu!(n-\nu)!} p^{\nu} q^{n-\nu} \tag{1}$$

where p is the probability of detecting a flare in one trial and q is the probability of no detection (1-p). Here we will refer to p as the duty cycle and note that in our context, this quantity describes what fraction of a set of 3-hr images should contain a flare. Figure 3 shows the probability distributions as a function of underlying duty cycle for both the X-ray experiment, in which ν=1 and n=7.6 (obtained by dividing the total time, 76 ksec, by the length of the observed X-ray flare, 10 ksec) and the near-infrared experiment, in which ν=0 and n=25. The X-ray and near-infrared probability distributions have only a small overlap, which suggests that if the flaring activity at X-ray and near-infrared wavelengths are coupled, a flare most likely occurred during the near-infrared experiment. The joint probability distribution quantifies this and suggests there is, at most, a probability of 9% of a random 3-hr near-infrared flare in excess of 19 mJy (dereddened). We therefore assume that at the 2σ confidence level, a flare occurred during our experiment and use our limits to constrain the variability models.

While only a limited amount of modeling of the recent 3-hr X-ray flare detected at Sgr A* has been carried out, existing models predict 2μm dereddened emission as high as 300 mJy in the model preferred by Markoff et al. (2001) but as small as 0.4 mJy in Liu & Melia (2002). The former model explains the elevated X-ray emission, produced by synchrotron self-Compton, by an enhanced temperature for the relativistic electron population, as might arise in a magnetic reconnection event. On the other hand, Liu & Melia present a flare model in which the flare arises due to an enhanced accretion rate and bremsstrahlung emission is dominant at both near-infrared and X-ray wavelengths. The lack of a near-infrared detection of Sgr A* makes the Markoff et al. (2001) model and any other mechanism that produces flared 2μm emission in excess of 19 mJy (dereddened) unlikely.

5. Conclusions

This paper summarizes a search for a near-infrared counterpart to Sgr A* in the flared state. From the length of our observations, this search was sensitive to variability on time scales of 3 hours. No such counterpart was detected. However, by identifying and removing all the stars in the crowded inner $\sim 0\farcs6 \times 0\farcs6$ of the Galactic Center, an upper limit for the emission from Sgr A* has been inferred for each observation epoch. These limits constrain the quiescent emission from Sgr A* to $\lesssim$0.09 mJy (2.0 mJy, dereddened) and the variable component to $\lesssim$0.8 mJy (19 mJy, dereddened) at the 2σ confidence level. More X-ray data will improve the estimated flaring duty cycle and is likely to increase the confidence level of our limits for the near-infrared component of the flared emission.

Valuable input on the manuscript was contributed by Gaspard Duchêne, Caer McCabe, and Andreas Eckart. Data presented herein were obtained at the W.M. Keck Observatory, which is operated as a scientific partnership among the California Institute of Technology, the University of California and the National Aeronautics and Space Administration. The Observatory was made possible by the generous financial support of the W.M. Keck Foundation. This work was supported by the NSF both through grant No. 9988397 and the Science and Technology Center for Adaptive Optics, managed by the University of California at Santa Cruz under cooperative agreement No. AST - 9876783. AMG also thanks the Packard Foundation for its support.

REFERENCES

Baganoff, F. K. et al. 2001a, Nature, 413, 45

Baganoff, F. K. et al. 2001b, ApJ, submitted (astro-ph/0102151)

Blum, R. D., Sellgren, K., & Depoy, D. L. 1996, ApJ, 470, 864

Christou, J. C. 1991, PASP, 103, 1040

Close, L. M., McCarthy, D. W., & Melia, F. 1995, ApJ, 439, 682

Diolaiti, E., Bendinelli, O., Bonaccini, D., Close, L., Currie, D., & Parmeggiani, G. 2000, A&AS, 147, 335

Eckart, A. & Genzel, R. 1997, MNRAS, 284, 576

Eckart, A., Genzel, R., Hofmann, R., Sams, B. J., & Tacconi-Garman, L. E. 1995, ApJ, 445, L23

Genzel, R. & Eckart, A. 1999, ASP Conf. Ser. 186: The Central Parsecs of the Galaxy, 3

Genzel, R., Eckart, A., Ott, T., & Eisenhauer, F. 1997, MNRAS, 291, 219

Genzel, R., Pichon, C., Eckart, A., Gerhard, O. E., & Ott, T. 2000, MNRAS, 317, 348

Gezari, S., Ghez, A. M., Becklin, E. E., Larkin, J., McLean, I. S., Morris, M. (2002), ApJ, in press (astro-ph/0205186)

Ghez, A. M., Klein, B. L., Morris, M., & Becklin, E. E. 1998, ApJ, 509, 678

Ghez, A. M., Morris, M., Becklin, E. E., Tanner, A., & Kremenek, T. 2000, Nature, 407, 349

Ghez, A. M. et al. 2002, in preparation

Herbst, T. M., Beckwith, S. V. W., & Shure, M. 1993, ApJ, 411, L21

Liu, S. & Melia, F. 2002, ApJ, 566, L77

Markoff, S., Falcke, H., Yuan, F., & Biermann, P. L. 2001, A&A, 379, L13

Matthews, K., Ghez, A. M., Weinberger, A. J., & Neugebauer, G. 1996, PASP, 108, 615

Matthews, K. & Soifer, B.T. 1994, Infrared Astronomy with Arrays: The Next Generation, I. McLean ed. (Dordrecht: Kluwer Academic Publishers), 239

McLean, I. S. et al. 1998, Proc. SPIE, 3354, 566

Melia, F. & Falcke, H. 2001, ARA&A, 39, 309

Menten, K. M., Reid, M. J., Eckart, A., & Genzel, R. 1997, ApJ, 475, L111

Morris, M., Tanner, A. M., Ghez, A. M., Becklin, E. E., Cotera, A., Werner, M. W., & Ressler, M. E. 2001, American Astronomical Society Meeting, 198, 4101

Rieke, G. H. & Lebofsky, M. J. 1985, ApJ, 288, 618

Stolovy, S. R., McCarthy, D. W., Melia, F., Rieke, G., Rieke, M. J., & Yusef-Zadeh, F. 1999, ASP Conf. Ser. 186: The Central Parsecs of the Galaxy, 39

Wizinowich, P. L. et al. 2000, PASP, 112, 315

Wizinowich, P. L. 2000, Proc. SPIE, 4007,

Zhao, J., Bower, G. C., & Goss, W. M. 2001, ApJ, 547, L29

Table 1. Near-Infrared Limits on Sagittarius A*

			PSF Characteristics			
Epoch (UT)	Camera	# frames	FWHM$_{core}$ ($''$)	FWHM$_{halo}$ ($''$)	E$_{core}$ (%)[a]	Limit (mag)[b]
1995 Jun 11	NIRC	2716	0.05	0.3	3	15.87
1996 Jun 25	NIRC	3866	0.06	0.5	1	13.71[c]
1996 Jun 27	NIRC	1600	0.06	0.4	2	14.73
1997 May 14	NIRC	2800	0.05	0.2	1	15.67
1998 Apr 2	NIRC	2744	0.05	0.4	2	15.01
1998 May 14	NIRC	3436	0.05	0.4	1	14.79
1998 May 15	NIRC	6468	0.05	0.3	2	16.31
1998 Aug 4	NIRC	4241	0.05	0.4	2	15.33
1998 Aug 5	NIRC	6272	0.05	0.3	3	16.62
1999 May 2	NIRC	7722	0.05	0.2	2	15.96
1999 May 3	NIRC	1764	0.05	0.2	2	15.85
1999 May 4	NIRC	1960	0.05	0.3	2	15.36
1999 May 27	KCAM+AO	15	0.08	0.2	38	17.02
1999 Jun 28	KCAM+AO	58	0.08	0.2	41	16.94
1999 Jul 24	NIRC	5677	0.05	0.2	4	17.17
1999 Jul 24	KCAM+AO	43	0.11	0.2	35	16.33
2000 Apr 21	NIRC	2744	0.05	0.5	1	14.20[c]
2000 May 19	NIRC	8232	0.05	0.3	3	16.43
2000 May 20	NIRC	6860	0.05	0.2	4	16.53
2000 Jun 21	SCAM+AO	215	0.08	0.2	26	15.41
2000 Jun 22	SCAM+AO	54	0.08	0.2	24	16.84
2000 Jul 19	NIRC	5473	0.06	0.3	4	16.24
2000 Jul 20	NIRC	3255	0.06	0.3	5	16.35
2000 Oct 18	NIRC	2286	0.05	0.3	2	15.73
2001 May 9	NIRC	6427	0.05	0.3	3	17.03
2001 Jul 28	NIRC	5684	0.05	0.2	5	16.61
2001 Jul 29	NIRC	3920	0.05	0.3	3	16.04

[a]Percentage of total energy contained in the PSF core

[b]Column 7 lists observed limits and column 8 lists dereddened values using an A_v=30 with A_k/
$A_{k'}/A_v$=0.117 (Melia & Falcke 2001; Rieke & Lebofsky 1985)

[c]Limits for the two images with halo FWHM $\geq 0\farcs5$ are not included in the analysis (see §3.2).

Fig. 1.— Speckle (left) and adaptive optics (right) images from May 1999 of the Galactic Center. The small box indicates a $1'' \times 1''$ region centered on Sgr A*, whose approximate position is marked with a cross. Both images are displayed with a histogram equalization stretch to show the fainter stars in the field and are oriented such that North is up and East is to the left.

Fig. 2.— The 3σ limiting flux density calculated for Sgr A* for each epoch of observation (corrected for reddening by a factor of $\sim$22.) The lowest limit of 2.0 mJy, a factor of two lower than previously published limits, and the highest limit of 19 mJy, constrains Sgr A*'s quiescent and variable states, respectively.

Fig. 3.— The probability (P_n) of seeing the number of detected flares (ν) of both this study (0 detections) and the Chandra experiment (1 detection; Baganoff et al. 2001a) for various duty cycles. The low joint probability suggests that if the flaring activity at near-infrared and X-ray wavelengths are coupled, a flare occurred during the near-infrared experiment and is restricted to be lower than our detection limit.

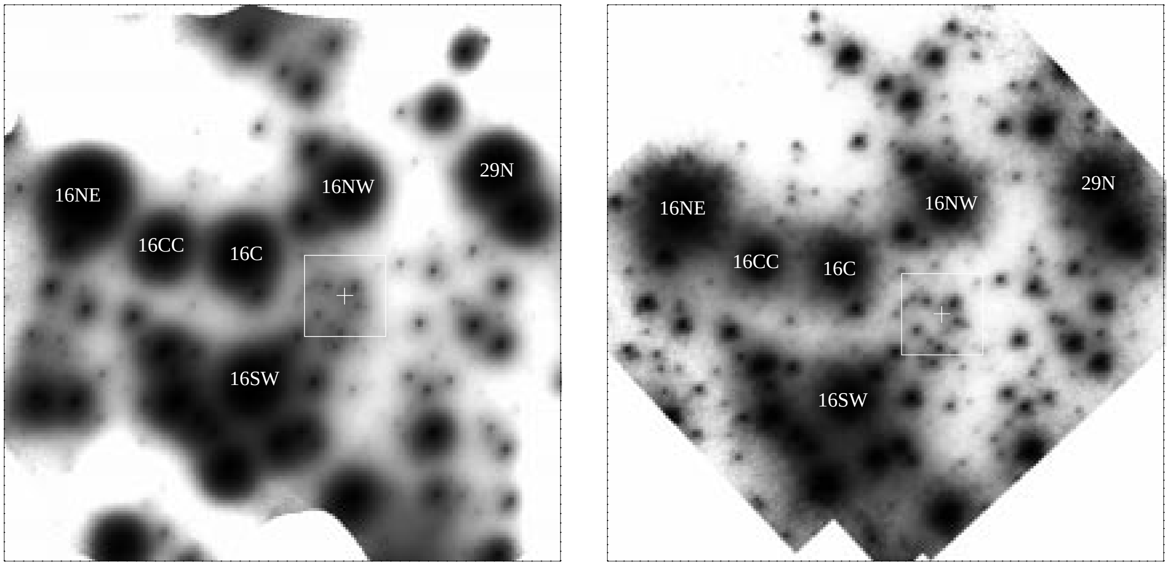
16NE
16CC
16C
16NW
29N
16SW
16NE
16CC
16C
16NW
29N
16SW

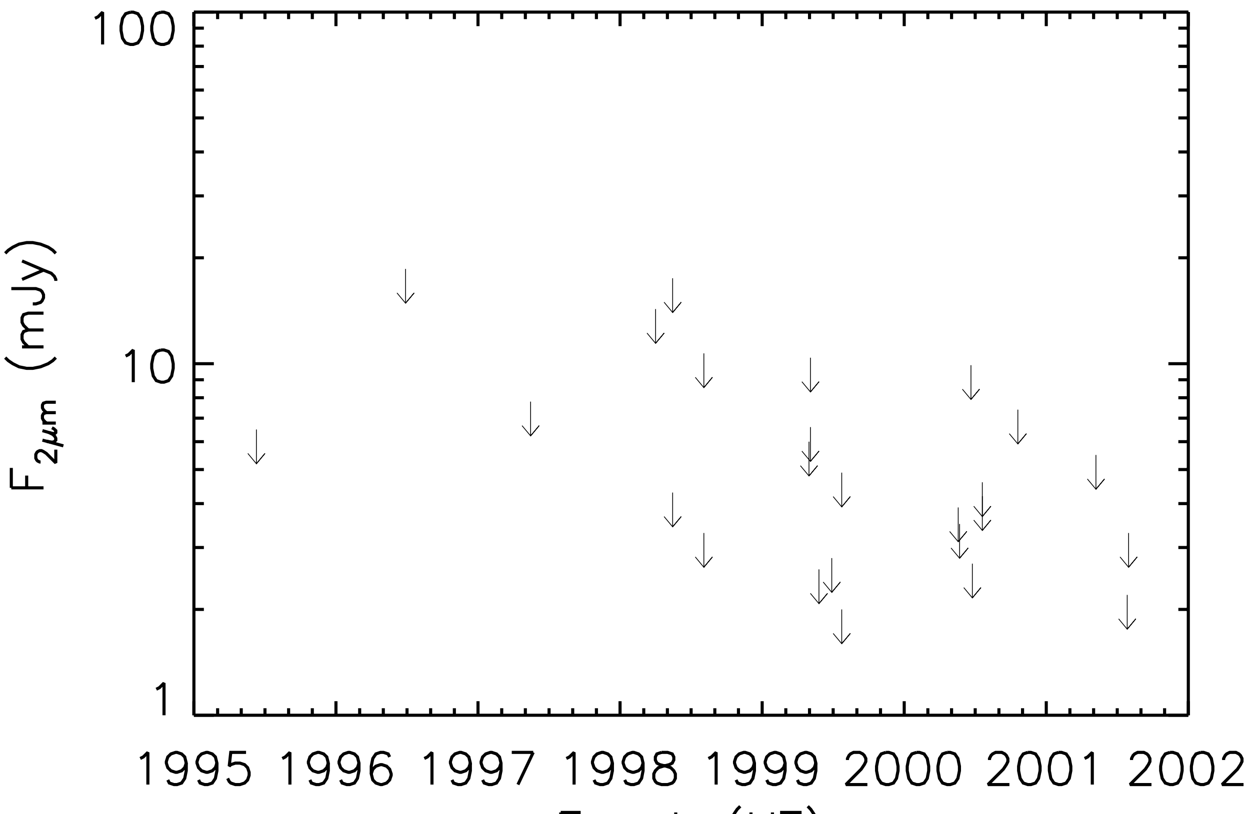
100
10
1
1995
1996
1997
1998
1999
2000
2001
2002
Epoch (UT)
$F_{2\mu m}$ (mJy)

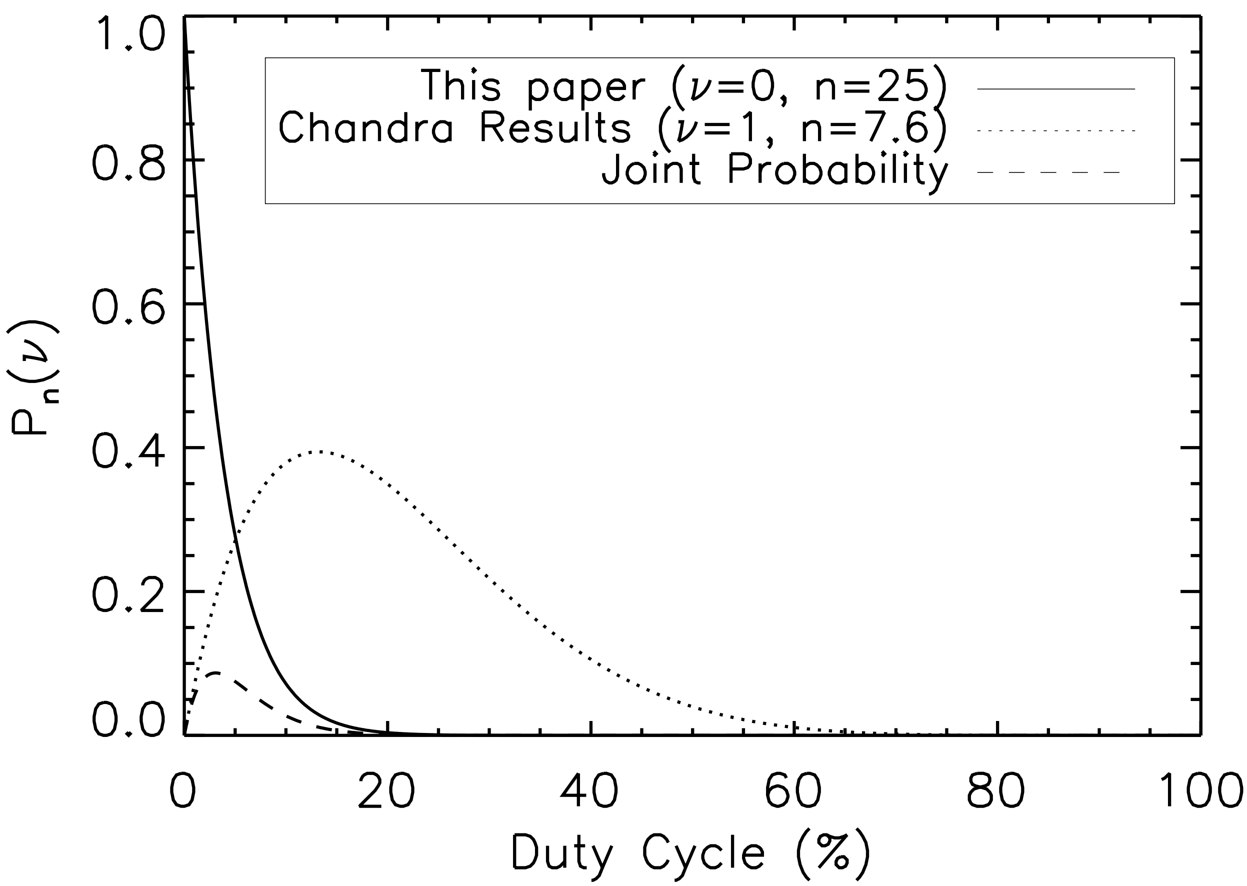
1.0
0.8
0.6
0.4
0.2
0.0
$P_n(\nu)$
0
20
40
60
80
100
Duty Cycle (%)
This paper (ν=0, n=25)
Chandra Results (ν=1, n=7.6)
Joint Probability